2018 European Control Conference (ECC)
June 12-15, 2018. Limassol, Cyprus

Semiglobal Feedback Linearization of the Human Head and Binocular Eye Tracking Dynamics Satisfying Donders' Law

Bijoy K. Ghosh[1] and Bhagya U. Athukorallage[1]

***Abstract*— In this paper, we revisit the head and binocular eye pointing control problems as a constrained dynamics on $SO(3)$ from the point of view of a nonlinear multi input multi output (MIMO) system. The constraint, proposed by Donders, is that for every human head rotating away from its primary pointing direction, the rotational vectors are restricted to lie on a surface called the Donders' surface. This paper assumes that the Donders' surface is described by a quadratic equation on the coordinates of the rotation vector. The inputs to the MIMO system are three external torques provided by muscles rotating the head. The three output signals are chosen as follows. Two of the signals are coordinates of the frontal pointing direction. The third signal measures deviation of the state vector from the Donders' surface. Thus we have a 3×3 square system and recent results have shown that this system is feedback linearizable on a suitable neighborhood $\mathscr{N}$ of the state space. In this paper, we estimate a lower bound on the size of $\mathscr{N}$ by computing a lower bound on the distance between the Donders' and the Singularity surface. For the eye pointing control, the Donders' surface is replaced by Listing's plane whereas the two eyes are constrained by a coplanarity condition. The binocular eye pointing control system is described as a MIMO system on $\mathbf{SO} = SO(3)\times SO(3)$ with six inputs and six outputs. Semiglobal feedback linearization, on a suitable neighborhood $\mathscr{B}$ of SO is proposed and an analogous lower bound on this neighborhood is obtained. Binocular tracking control using semiglobal feedback linearization, described in this paper, is new.**

I. INTRODUCTION

The subject matter of this paper is to control the pointing direction of a rigid body, such as the human eye or the head (see Robinson [1] and Peng et. al. [2]). The control inputs are generated by external torques from a set of muscles rotating the rigid body. The goal is to make the 'pointing direction' (for example, the nose direction of the head or the gaze direction of the eye) of the body directed towards a point target. If this target is moving along a path already predefined in $\mathbb{R}^3$, then the 'body pointing direction' needs to track the direction of the point target, in order to keep the 'target in view'. Even after pointing towards a target, the orientation of the eye/head being controlled remains ambiguous and the 'eye/head movement controller' disambiguates the orientation by imposing additional constraint on the rotation vector (a vector along the axis of rotation). Such constraints were originally proposed (for both the eye and the head movement problems) in 1845 by physiologists such as Listing, Donders and Helmholtz, among others [3]. In the case of head movement, this constraint is popularly known as the Donders' constraint (Listing's constraint in the case of eye movement [4], [5]). The Donders' surface (see [6] for a picture and a precise mathematical definition[1]) is considered to be a fixed surface but changes from one human being to another.

Recall from [7] that in a neighborhood of the space of allowed orientations constrained by Donders' and Listing's constraints, one can 'locally linearize' the 'rotation dynamics' by a static state feedback. The linear system, we have seen, has two components. The first one is transverse to the constraint-surface and the second one is tangential. For the head movement problem, asymptotic stability of the transverse component guarantees (Donders') constraint satisfaction. For the monocular eye movement problem asymptotic stability, likewise, would guarantee Listing's constraint satisfaction. In this paper, we extend our results to the binocular eye movement problem, where asymptotic stability would additionally guarantee that the eye gazes meet at a point, as would be the case when the two eyes focus on a point target.

II. SO(3) AND THE QUATERNION CONNECTION

Some of the main ideas are sketched here from [7] for notational details. In the following, we introduce the space $\mathbf{SO}(\mathbf{3})$ of orthogonal matrices and its connection to the space of unit quaternion[2].

A. Head/Eye orientation as a subset of SO(3)

Let R be a point in $\mathbf{SO}(\mathbf{3})$ with column vectors denoted by $R_i, i = 1,2,3$. Columns of R can be associated with a frame attached to the head/eye and would therefore correspond to a specific orientation. Let us denote by $\{r_{ij}\}_{i,j=1,2,3}$ the components of the rotation matrix R. R_1 would be called the 'head pointing direction' or the 'eye gaze direction'. R_3 would be called the 'top direction', which indicates if the head/eye is tilting towards the left or right. We consider the head/eye orientation in the right-handed system, denoted by symbol X-Y-Z, in $\mathbb{R}^3$. As in [7], the head/eye orientation is confined to a subset of $\mathbf{SO}(\mathbf{3})$ given by $\mathscr{H} := \{R \in \mathbf{SO}(\mathbf{3}) \,|\, \text{trace}(R) > 0 \text{ and } r_{11} > 0\}$.

*Supported in part by Dick and Martha Professorship at Texas Tech University, Lubbock, USA

[1]Bijoy K. Ghosh and Bhagya U. Athukorallage are with Department of Mathematics and Statistics, Texas Tech University, Lubbock, 79409-1042, USA bijoy.ghosh@ttu.edu; bhagya.athukorala@ttu.edu

[1]Donders' surface constraint restricts the degree of freedom for head movement from 3 to 2. For eye movement, the corresponding Listing's constraint, would restrict rotation of human eye about the direction of gaze.

[2]This connection is a well established fact in the literature (see [8], [3] for references).

B. Some formula on $\mathscr{H}$ and quaternion connection

It turns out that the axis of rotation $\bar{n}$, for the rotation matrix R, can be written as

$$\bar{n} := \begin{bmatrix}\bar{n}_1 & \bar{n}_2 & \bar{n}_3\end{bmatrix}^T = \frac{1}{2\sin\alpha}\begin{bmatrix} n_1 & n_2 & n_3\end{bmatrix}^T, \tag{1a}$$

$$n := \begin{bmatrix} n_1 & n_2 & n_3\end{bmatrix}^T = \begin{bmatrix} r_{32}-r_{23}, r_{13}-r_{31}, r_{21}-r_{12}\end{bmatrix}^T \tag{1b}$$

The variable α is the counterclockwise rotation angle about the rotational axis $\bar{n}$. Associated with a rotation matrix R, there is a unit quaternion $q = [q_0 \;\; q_1 \;\; q_2 \;\; q_3]^T \in \mathbb{S}^3$. This quaternion connection is well known in the literature (see [9]). As in [7], we now consider a parametrization of unit quaternion proposed by Novelia and O'Reilly [10], [11], given by

$$q(\psi,\phi_1,\phi_2) := \tag{2}$$
$$[\cos\tfrac{\psi}{2}\cos\phi_1 \;\; \cos\tfrac{\psi}{2}\sin\phi_1 \;\; \sin\tfrac{\psi}{2}\cos\phi_2 \;\; \sin\tfrac{\psi}{2}\sin\phi_2]^T \in \mathbb{S}^3$$

where $\psi \in [0 \;\; \pi]$ and $\phi_1, \phi_2 \in [-\pi \;\; \pi)$. The vector R_1 is described using (2) as follows

$$R_1(\psi,\theta) = [\cos\psi \quad \sin\psi\sin\theta \quad -\sin\psi\cos\theta]^T, \tag{3}$$

where we define a new angle parameter $\theta := \phi_1 + \phi_2 \in [-\pi \;\; \pi)$. It is easy to see that $r_{11} = \cos\psi > 0$ if $0 \le \psi < \frac{\pi}{2}$. It follows that, for a fixed value of ψ, $l^2 = r_{21}^2 + r_{31}^2 = \sin^2\psi$, i.e, the pointing directions (r_{21}, r_{31}) are points on the circle with radius $l = \sin\psi \ge 0$ with the angle measure θ.

III. Quadratic Donders' Constraint

Donders' constraint in a quadratic polynomial form was originally introduced in [12], [13] and describes a quadratic surface using quaternion parameters q_0, q_1, q_2, q_3. These surfaces were subsequently used by the first author in [3] and [6] for the study of human head movement problems. In this paper, we consider a simplified form of the quadratic Donders' surface given by

$$q_0 q_1 = h_D(q_2, q_3), \tag{4}$$

where we define the polynomial h_D as

$$h_D(q_2,q_3) \;:=\; c_{22}q_2^2 + c_{23}q_2q_3 + c_{33}q_3^2. \tag{5}$$

Remark 3.1: The simplified Donders' surface (4) contains Listing's plane and the surfaces generated from Fick's and Helmholtz's gimbals, as a special case. Our motivation to consider this simplification is that the relative degree computations in section IV is well defined entirely over a suitably chosen open set $\mathscr{N}$.

We proceed to describe a theorem which shows that for a sufficiently small choice of the angle variable ψ, there exists orientations in $\mathscr{H}$ that satisfies (4). Rewriting (4) in terms of the parametrization (2) we obtain $h_D := \bar{h}_D(\phi_2)\left[\sin^2\frac{\psi}{2}\right]$, where

$$\bar{h}_D(\phi_2) := \frac{1}{2}[(c_{22}+c_{33}) + (c_{22}-c_{33})\cos 2\phi_2 + c_{23}\sin 2\phi_2].$$

We continue to assume that ψ is restricted to the interval $[0 \;\; \frac{\pi}{2})$, in order to ensure that $r_{11} = \cos\psi > 0$. We also have a bound $|\bar{h}_D(\phi_2)| < C$, for all ϕ_2 in the closed interval $[-\pi, \pi)$ where the constant C is assumed to satisfy

$$C \;>\; \tfrac{1}{2}|c_{22}+c_{33}| + \tfrac{1}{2}\sqrt{(c_{22}-c_{33})^2 + c_{23}^2}. \tag{6}$$

We now define a constant $\bar{\psi}$ as follows.

$$\bar{\psi} \;:=\; \begin{cases} 2\arctan(\frac{1}{\sqrt{2C}}) & \text{if } 2C \ge 1, \\ \frac{\pi}{2} & \text{otherwise.} \end{cases} \tag{7}$$

We now state without details of the proof, the following theorem from [7].

Theorem 3.1: Assume that c_{22}, c_{23}, and c_{33} be specified fixed parameters of $h_D(q)$ in (5) describing the corresponding Donders' constraint. Let us define $\bar{\psi}$ as in (7) and choose $\psi \in [0 \;\; \bar{\psi})$. Then for a given pointing direction in the form $p = R_1(\psi,\theta)$ from (3) where $\theta \in [-\pi \;\; \pi)$, there exist an unique orientation matrix $R \in \mathscr{H}$ in the form $R = [p, R_2, R_3]$ that satisfies the Donders' constraint (4).

Proof: The details of the proof is omitted. The main point is that when $0 \le \psi < \bar{\psi}$ and $-\pi \le \theta < \pi$, the equation

$$\sin(2\phi_1) \;=\; 2\tan^2\frac{\psi}{2}\,\bar{h}_D(\theta - \phi_1) \tag{8}$$

can be solved uniquely for ϕ_1 in the interval $(-\frac{\pi}{4} \;\; \frac{\pi}{4})$. ■

IV. A Dynamical System for Eye/Head Rotation

We start this section by describing a subset $\mathscr{H}_{\bar{\psi}}$ of $\mathbf{SO(3)}$. Let $\bar{\psi}$ be as described in (7), we define

$$\mathscr{H}_{\bar{\psi}} := \left\{R \in \mathscr{H} \,|\, r_{21}^2 + r_{31}^2 < \sin^2\bar{\psi}\right\}.$$

Intuitively, $\mathscr{H}_{\bar{\psi}}$ contains all orientation matrices in $\mathscr{H}$ whose pointing direction vectors are in the allowed region prescribed by Theorem 3.1. We now describe a rotating rigid body dynamics on $\mathscr{H}_{\bar{\psi}}$ and show that such a dynamics is feedback linearizable by a static state feedback in the neighborhood of the Donders' surface. The rigid body dynamics and the output vector are described in the following subsection.

A. A rigid body dynamics with Donders' constraint

Let us consider the following rigid body dynamics [14], [15] of the human head in the 'inertial frame'

$$\dot{R}(t) \;=\; -R(t)\hat{\omega}(t), R \in \mathscr{H}_{\bar{\psi}}, \tag{9}$$

$$J\,\dot{\omega}(t) \;=\; \hat{\omega}\,J\,\omega + T, \tag{10}$$

where $J = \mathrm{diag}\{J_1, J_2, J_3\}$ is the moment of inertia matrix, $J_i > 0$, $i = 1,2,3$; $T \in \mathbb{R}^3$ are externally applied control torques; and $\omega = [\omega_1, \omega_2, \omega_3]^T \in \mathbb{R}^3$ is the angular velocity vector[3]. We define

$$\hat{\omega} = \begin{bmatrix} 0 & \omega_3 & -\omega_2 \\ -\omega_3 & 0 & \omega_1 \\ \omega_2 & -\omega_1 & 0 \end{bmatrix}. \tag{11}$$

The Donders' constraint (4) can be written as

$$n_1 = \mathscr{D}(n_2, n_3) = \mathscr{T}^{-1}\left(c_{22}n_2^2 + c_{23}n_2n_3 + c_{33}n_3^2\right), \tag{12}$$

[3] The underlying state space of the dynamical system (9), (10) is $\tilde{\Xi} = \mathscr{H}_{\bar{\psi}} \times \mathbb{R}^3$, a 6 dimensional manifold.

where n_1, n_2, n_3 have been defined in (1b), $\mathscr{T} = trace(R)+1$. An output function

$$y = [h_1, h_2, h_3]^T = [r_{21},\ r_{31},\ \mathscr{D}(n_2, n_3) - n_1]^T \in \mathbb{R}^3. \quad (13)$$

is now introduced. Let us now define a proper subset $\mathscr{H}_{\Psi}^D$ as follows $\mathscr{H}_{\Psi}^D := \left\{ R \in \mathscr{H}_{\Psi} \,|\, n_1 = \mathscr{D}(n_2, n_3) \right\}$. The subset $\mathscr{H}_{\Psi}^D$ contains all orientation matrices in $\mathscr{H}_{\Psi}$ that satisfies Donders' constraint (12). For notational convenience, we define $\Xi^D = \mathscr{H}_{\Psi}^D \times \mathbb{R}^3$, and define $\mathscr{N}$ to be a small enough open neighborhood of Ξ^D inside $\widehat{\Xi}$.

The dynamical system (9), (10), (13) can be written as a control-affine nonlinear 3-input 3-output system defined on $\mathscr{N}$ as follows

$$\dot{x} \ = \ f(x) + \sum_{i=1}^{3} g_i(x) u_i, \quad (14a)$$

$$y_i \ = \ h_i(x),\ i = 1,2,3, \quad (14b)$$

where f and g are smooth vector fields $\mathscr{N} \to \mathbb{R}^6$, and all h_i are smooth scalar functions $\mathscr{N} \to \mathbb{R}$. Note that x abstractly denotes the state variable $(\psi, \theta, \phi_1, \omega_1, \omega_2, \omega_3)$ of the dynamical system.

B. Preliminary remarks from nonlinear MIMO control

For standard definition of vector relative degree and decoupling matrix see [16], [20]. We shall write the decoupling matrix

$$N(x) \ := \ \begin{pmatrix} L_{g_1} L_f^{r_1 - 1} h_1 & \cdots & L_{g_3} L_f^{r_1 - 1} h_1 \\ \vdots & \ddots & \vdots \\ L_{g_1} L_f^{r_3 - 1} h_3 & \cdots & L_{g_3} L_f^{r_3 - 1} h_3 \end{pmatrix} \in \mathbb{R}^{3 \times 3}. \quad (15)$$

We note from [7] that the dynamical system (9), (10) and (13) has a vector relative degree $[2,2,2]$ at every point on $\mathscr{N}$ and the decoupling matrix (15) is a 3×3 matrix of rank 3 everywhere on $\mathscr{N}$.

C. Main theorem

Theorem 4.1: ([7]) On a small neighborhood of every point on $\mathscr{N}$, there exist a static feedback law $u^* := a(x) + b(x)v$ such that the rigid body dynamics (9), (10) with output (13) is feedback equivalent to the following controllable linear systems

$$\ddot{z}_i = v_i \text{ for } i = 1,2, \quad (16)$$

$$\dddot{\xi} = v_3, \quad (17)$$

where $v \in R^3$ is the new control input vector and new output variables are defined by

$$\left[z_1 \ z_2 \ \xi \right]^T := h = \left[r_{21} \ r_{31} \ \mathscr{D}(n_2, n_3) - n_1 \right]^T. \quad (18)$$

For the proof, see [7].

D. Proof of Theorem 4.1

Proof: According to Theorem 3.1 in [17] (see also [16]), we need to show that the output h in (13) has a vector relative degree defined uniformly on Ξ^D. In order to calculate the relative degree, we need to compute Lie derivatives of h up to second order [16]. The details of the Lie derivative computations have been omitted.

It is easy to see that $L_{g_i} h_j = 0$ for $i, j = 1,2,3$. The decoupling matrix N in (15) is given by

$$N(x) \ = \ \begin{bmatrix} 0 & -r_{23} J_2^{-1} & r_{22} J_3^{-1} \\ 0 & -r_{33} J_2^{-1} & r_{32} J_3^{-1} \\ L_{g_1} L_f h_3 & L_{g_2} L_f h_3 & L_{g_3} L_f h_3 \end{bmatrix}. \quad (19)$$

Using the identity $r_{11} = r_{22} r_{33} - r_{23} r_{32}$, it follows that $\det N(x) = r_{11} J_2^{-1} J_3^{-1} L_{g_1} L_f h_3(x)$. We claim [7] that $L_{g_1} L_f h_3(R)|_{\mathscr{H}_{\Psi}^D} < 0$ so that $\det N(x) \neq 0$ on $\mathscr{H}_{\Psi}^D$. It follows that the output h has uniformly, the relative degree $[2,2,2]$ on $\mathscr{H}_{\Psi}^D$ and we would have the following local diffeomorphism and feedback law

$$[z_1,\ z_2,\ z_3,\ z_4,\ \xi_1,\ \xi_2] = \mathbf{\Phi}(\psi, \theta, \phi_1, \omega) \ = \ [h_1, h_2, L_f h_1, L_f h_2, h_3, L_f h_3] \quad (20)$$

where $z_3 = \dot{z}_1, z_4 = \dot{z}_2$, and $\xi_2 = \dot{\xi}_1$,[4] and

$$a(x) \ := \ N^{-1}(x) [L_f^2 h_1 L_f^2 h_2 L_f^2 h_3]^T \text{ and } b(x) \ := \ N^{-1}(x). \quad (21)$$

This would render the rigid body dynamics in (9), (10) locally feedback equivalent to the linear system in (16), (17), on Ξ^D. ■

Remark 4.1: The linearization method adopted in this paper from [7] has been proposed in [17], [18] in order to decompose the system dynamics into a tangential part and a part transverse to the Donders' submanifold (4).

From what we have presented so far, the mapping $\mathbf{\Phi}$ from $\mathscr{N} \to \mathbf{\Phi}(\mathscr{N}) \subset \mathbb{R}^6$, is a local diffeomorphism. We now claim (following a theorem due to Hadamard [19]) that if $\mathscr{N}$ is such that

$$\| \left[\mathbf{\Phi}'(x) \right]^{-1} \| \ \leq \ M \quad (22)$$

for all $x \in \mathscr{N}$ and for a fixed real number M, then the diffeomorphism $\mathbf{\Phi}$ is global.

Remark 4.2: Hadamard's main argument is that if $\mathbf{\Phi}$ is a local homeomorphism, then $\mathbf{\Phi}$ is a global homeomorphism if $\mathbf{\Phi}$ lifts line segments (see [19], page 219) and the range of $\mathbf{\Phi}$ is simply connected[5]. A sufficient condition for $\mathbf{\Phi}$ to lift line segments is (22). In fact the line segment is constructed by solving an initial value problem described in [19], page 221.

V. Sketches of the Donders' and Singularity Surfaces

The purpose of this section is to numerically visualize how large we can choose the neighborhood $\mathscr{N}$. It would follow from (22) that $\mathscr{N}$ should be chosen as a simply connected domain of $\mathbb{R}^6$ large enough so that the inequality constraint (22) is satisfied. We now proceed to plot the Donders' surface and the Singularity surface for the decoupling matrix (19) and the jacobian matrix $\mathbf{\Phi}'(x)$. Recall that the Donders' surface is the set of points in the (ψ, θ, ϕ_1) space that satisfy (8). Explicit computation shows that (8) can be rewritten as

[4] Note that $\xi_1 = \xi$, as in (18).

[5] If we assume that $\mathscr{N}$ is a simply connected domain of $\mathbb{R}^6$, then assuming (22) $\mathbf{\Phi}(\mathscr{N})$ is also simply connected. This is because the pair $(\mathscr{N}, \mathbf{\Phi})$ covers $\mathbf{\Phi}(\mathscr{N})$. It would follow that any path γ in $\mathbf{\Phi}(\mathscr{N})$ can be lifted to a path in $\mathscr{N}$, which can be shrunk to a point. This would imply that γ can also be shrunk to a point.

$$\sin\left(2\phi_1\right) - \tan^2\left(\frac{\psi}{2}\right)\left[(c_{22}-c_{33})\cos(2(\theta-\phi_1))+ c_{23}\sin(2(\theta-\phi_1)) + c_{22}+c_{33}\right] = 0, \quad (23)$$

where $\phi_1 \in (-\frac{\pi}{4}, \frac{\pi}{4})$, $\theta \in [-\pi, \pi)$, and $\psi \in (0, \bar{\psi})$ with $\bar{\psi}$ defined in (7). Determinant of the decoupling matrix $N(x)$ given by (19) is of the form $-(2J_1J_2J_3)^{-1}\cos(\psi)\,\Upsilon$, where

$$\begin{aligned}\Upsilon = \big[&(c_{22}-c_{33})[\sin(2\theta-\psi-2\phi_1)+\sin(2\theta+\psi-2\phi_1)]- \\ &2(c_{22}-c_{33})\sin(2(\theta-\phi_1)) - c_{23}\cos(2\theta-\psi-2\phi_1) - \\ &c_{23}\cos(2\theta+\psi-2\phi_1) + 2c_{23}\cos(2(\theta-\phi_1)) + \\ &\cos(\psi-2\phi_1)+\cos(\psi+2\phi_1)+2\cos(2\phi_1)\big]. \end{aligned} \quad (24)$$

Determinant of the Jacobian $\mathbf{\Phi}'(x)$ of the Output map $\mathbf{\Phi}$ (20), on the other hand, is given by $-\frac{1}{2}\sin(\psi)\cos^2(\psi)\,\Upsilon^2$. It would follow that, other than the two points $\psi = 0$ and $\psi = \pi/2$, [6] the decoupling matrix and the jacobian matrix are singular exactly on the surface

$$\Upsilon = 0, \quad (25)$$

which we shall call, the 'Singularity surface'. The Donders' surface (23) and the Singularity surface (25) are now plotted for four special cases in Fig. 1. To plot the surfaces in 2 dimension, we choose two specific values of ψ in Fig. 1 (This figure was also plotted in [20], without the explicit computation of critical points.).

In Figs. 1a and 1b, we have assumed that $c_{22} = 1, c_{23} = c_{33} = 0$ and $\bar{\psi} = 1.23096$ (corresponds to the Donders' surface $q_0q_1 = q_2^2$). In Figs. 1c and 1d, we have assumed that $c_{33} = 1, c_{23} = c_{22} = 0$ and $\bar{\psi} = 1.23096$ (corresponds to the Donders' surface $q_0q_1 = q_2^2$). In Figs. 1e and 1f, we have assumed that $c_{22} = c_{33} = 0, c_{23} = -1$ and $\bar{\psi} = \frac{\pi}{2}$. This is the well known Fick-Gimbal (corresponds to the Donders' surface $q_0q_1 = -q_2q_3$). Finally in Figs. 1g and 1h, we have assumed that $c_{22} = c_{33} = 0, c_{23} = 1$ and $\bar{\psi} = \frac{\pi}{2}$. This is the well known Helmholtz Gimbal (corresponds to the Donders' surface $q_0q_1 = +q_2q_3$).

VI. Critical points of the Donders' and Singularity Surfaces

A. Donders' surface

Consider the Donders' surface from (23) as follows

$$\sin(2\phi) - \tan^2\left(\frac{\psi}{2}\right)(a\cos(2\theta-2\phi)+b\sin(2\theta-2\phi)+c) = 0, \quad (26)$$

where, $a = c_{22}-c_{33}$, $b = c_{23}$, $c = c_{22}+c_{33}$, and $\phi = \phi_1(\theta)$ is viewed as a function of θ. Taking the derivative of ϕ with respect to the θ variable, one can show from (26) that the critical points exists at

$$b\cos(2\theta-2\phi) - a\sin(2\theta-2\phi) = 0. \quad (27)$$

Let us now define

$$\cos(2\theta-2\phi) = \lambda a \text{ and } \sin(2\theta-2\phi) = \lambda b, \quad (28)$$

where $\lambda = \pm\frac{1}{\sqrt{a^2+b^2}}$. Evaluating the Donder's surface (26) at the critical point, we obtain

$$\phi^* = \frac{1}{2}\sin^{-1}\left(\tan^2\left(\frac{\psi}{2}\right)\left(\lambda(a^2+b^2)+c\right)\right). \quad (29)$$

B. Singularity surface $\Upsilon = 0$

The Singularity surface $\Upsilon = 0$ from (25) is described by the equation:

$$\Upsilon = -\sin^2\left(\frac{\psi}{2}\right)[a\sin(2\theta-2\phi)-b\cos(2\theta-2\phi)] + \cos^2\left(\frac{\psi}{2}\right)\cos(2\phi) = 0, \quad (30)$$

where $a = c_{22}-c_{33}$, $b = c_{23}$ and $\phi = \phi_1(\theta)$ as in the previous subsection. Taking derivative of ϕ with respect to the θ variable, one can show that critical points of the surface (30) satisfy the condition:

$$a\cos(2\theta-2\phi) + b\sin(2\theta-2\phi) = 0. \quad (31)$$

We now define, as in (28), the following

$$\cos(2\theta-2\phi) = \lambda b \text{ and } \sin(2\theta-2\phi) = -\lambda a, \quad (32)$$

where $\lambda = \pm\frac{1}{\sqrt{a^2+b^2}}$. Hence, at a critical point, the Singularity surface takes the value

$$\Upsilon^* = \sin^2\left(\frac{\psi}{2}\right)\lambda(a^2+b^2) + \cos^2\left(\frac{\psi}{2}\right)\cos(2\phi^*) = 0,$$

and we compute

$$\phi^* = \frac{1}{2}\cos^{-1}\left(-\tan^2\left(\frac{\psi}{2}\right)\lambda(a^2+b^2)\right). \quad (33)$$

Remark 6.1: Let us denote the critical angle ϕ^* from (29) as ϕ_D^* and the critical angle ϕ^* from (33) as ϕ_S^*, it would follow that

$$\sin(2\phi_D^*) = \tan^2\frac{\psi}{2}\left[c \pm \sqrt{a^2+b^2}\right] = y \quad (34)$$

and

$$\cos(2\phi_S^*) = \tan^2\frac{\psi}{2}\left[\pm\sqrt{a^2+b^2}\right] = x. \quad (35)$$

The vertical lines in Fig. 1 illustrate the critical points, $\{\phi_D^*, \phi_S^*\}$, of the Donders' and Singularity surfaces[7]. For any fixed value of ψ, a lower bound on the shortest distance between the Donders' surface (26) and the Singularity surface (30) is given by the smallest value of $\|\phi_D^* - \phi_S^*\|$, under the constraints (34) and (35). For four different examples of Donders' surfaces the actual distances between the Donders' surface and the Singularity surface is plotted in Fig.2. Using the critical points, a lower bound is now plotted in Fig. 3. In Fig.4a a comparison between the actual distance function and the corresponding lower bound from Figs 2a and 3a has been displayed. In Fig. 4b, the lower bound on the shortest distance is plotted as a function of two variables x and y. For a specific value of a, b and c, the lower bound function on the shortest distance between the Donders' surface (26) and the Singularity surface (30) can now be recovered from the surface in Fig. 4b.

[6] Whereas it is reasonable to assume that ψ is strictly less than $\frac{\pi}{2}$, excluding the straight gaze/pointing direction $\psi = 0$ is not so reasonable. However this is reminiscent of the Novelia and OReilly parametrization we have chosen. In fact for this parametrization, the corresponding Euler-Lagrange equation (see [8]) also has a singularity at the point $\psi = 0$.

[7] In order to capture all the critical points of the Donders' surface, it may be required to add an integral multiple of $\frac{\pi}{2}$ to the angle variable ϕ_S^*.

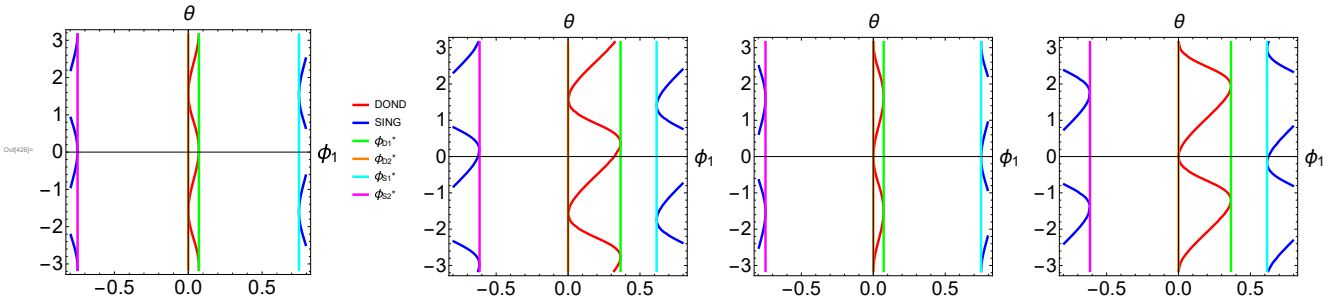

(a) $\psi = \frac{\pi}{6}$, Donders' surface $q_0q_1 = q_2^2$ (b) $\psi = \frac{\pi}{3}$, Donders' surface $q_0q_1 = q_2^2$ (c) $\psi = \frac{\pi}{6}$, Donders' surface $q_0q_1 = q_3^2$ (d) $\psi = \frac{\pi}{3}$, Donders' surface $q_0q_1 = q_3^2$

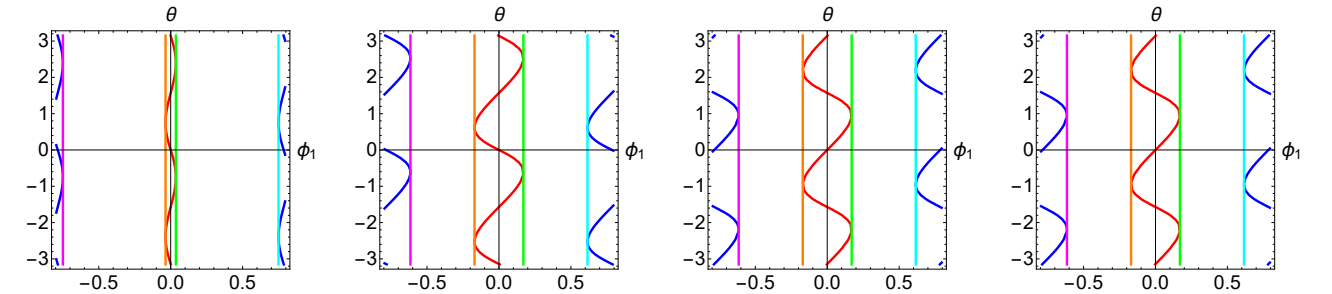

(e) $\psi = \frac{\pi}{6}$, Fick Gimbal $q_0q_1 = -q_2q_3$ (f) $\psi = \frac{\pi}{3}$, Fick Gimbal $q_0q_1 = -q_2q_3$ (g) $\psi = \frac{\pi}{6}$, Helmholtz Gimbal $q_0q_1 = +q_2q_3$ (h) $\psi = \frac{\pi}{3}$, Helmholtz Gimbal $q_0q_1 = +q_2q_3$

Fig. 1. The middle red curve is the Donders' surface (23) for a fixed value of ψ indicated in the caption. The blue curves are the Singularity surface (25), once again for a fixed value of ψ. The horizontal axis is the ϕ_1 variable in the interval $(-\frac{\pi}{4}, \frac{\pi}{4})$. The vertical axis is the θ variable in the interval $[-\pi, \pi)$. The vertical lines illustrate solutions of the constraints (34) and (35), and note that the subscripts $\{1, 2\}$ in ϕ^* denote the solutions that correspond to $+$ and $-$ signs in (34) and (35), respectively.

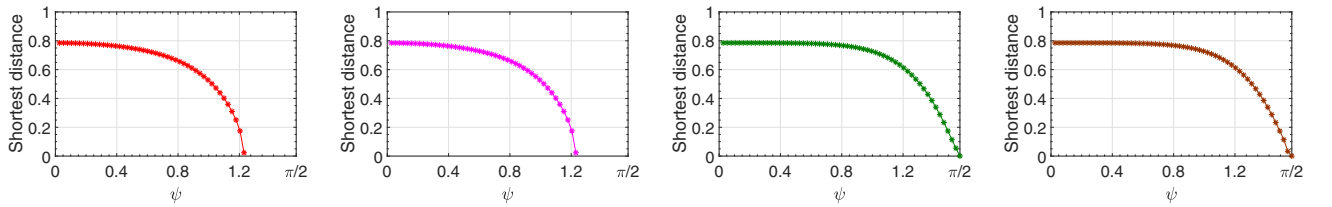

(a) Donders' case $q_0q_1 = q_2^2$, see Figs. 1a and 1b (b) Donders' case $q_0q_1 = q_3^2$, see Figs. 1c and 1d (c) Fick Gimbal $q_0q_1 = -q_2q_3$, see Figs. 1e and 1f (d) Helmholtz Gimbal $q_0q_1 = q_2q_3$, see Figs. 1g and 1h

Fig. 2. For a fixed value of ψ the shortest distance between the Donders' surface (23) and the Singularity surface (25) is plotted as ψ varies from 0 to the maximum value $\bar{\psi}$.

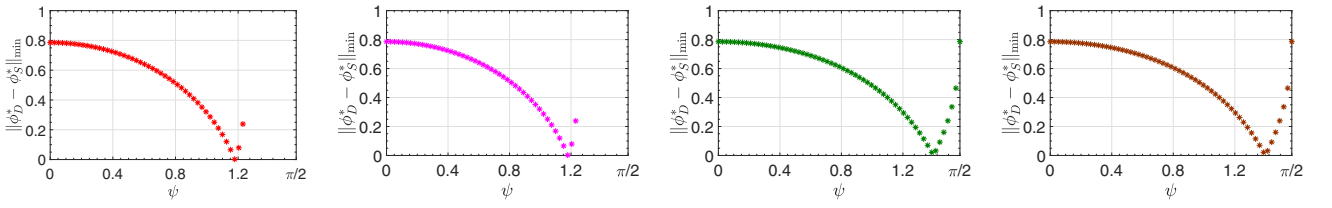

(a) Donders' case $q_0q_1 = q_2^2$, see Figs. 1a and 1b (b) Donders' case $q_0q_1 = q_3^2$, see Figs. 1c and 1d (c) Fick Gimbal $q_0q_1 = -q_2q_3$, see Figs. 1e and 1f (d) Helmholtz Gimbal $q_0q_1 = q_2q_3$, see Figs. 1g and 1h

Fig. 3. For a fixed value of ψ the lower bound on the shortest distance between the Donders' surface (23) and the Singularity surface (25) is plotted as ψ varies from 0 to the maximum value $\bar{\psi}$.

VII. The Binocular Eye Movement

We consider a pair of rigid spheres that model the two human eyes. We assume that the frames attached to the two eyes are aligned precisely as described in section II. The vector separating the centers of the two eyes are aligned along the Y-axis. The equation of motion for each of the two eyes are written in the inertial frame (see (9), (10)) as

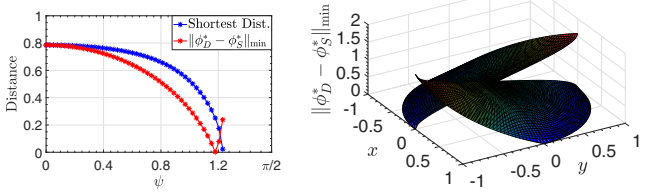

(a) (b)

Fig. 4. Figure 4a compares the shortest distance between the Donders' and Singularity surfaces with the corresponding lower bound $\|\phi_D^* - \phi_S^*\|_{\min}$ for the Donders' case $q_0 q_1 = q_2^2$. Figure 4b shows the variation of the lower bound on the distance between the Donders' and Singularity surfaces inside the unit disk $x^2 + y^2 \leq 1$. In this figure, we observe the lower bound $\|\phi_D^* - \phi_S^*\|_{\min} = 0$ along the boundary of the domain that corresponds to the first and third quadrants. Note that the angles ϕ_D^* and ϕ_S^* have opposite signs in the second and fourth quadrants, and hence, we observe discontinuities of the surface, $\|\phi_D^* - \phi_S^*\|_{\min}$, as we move across the quadrants I–II and III–IV.

follows. For $i = 1, 2$ we write

$$\dot{R}^i(t) \;=\; -\,R^i(t)\hat{\omega}^i(t), R^i \in \mathscr{H}_{\Psi}, \tag{36}$$

$$J^i\,\dot{\omega}^i(t) \;=\; \hat{\omega}^i\,J^i\,\omega^i + u^i \tag{37}$$

where $J^i = \text{diag}\left\{J_1^i, J_2^i, J_3^i\right\}$ is the moment of inertia matrix, $J_j^i > 0,\ j = 1,2,3$; $u^i \in \mathbb{R}^3$ are externally applied control torques; and $\omega^i = [\omega_1^i, \omega_2^i, \omega_3^i]^T \in \mathbb{R}^3$ is the angular velocity vector[8]. We define $\hat{\omega}^i$ as in (11). Let us now consider the output function

$$\begin{aligned} y &= h(R^1, R^2) = [h_1, h_2, h_3, h_4, h_5, h_6]^T \\ &= [r_{21}^1, r_{31}^1, \mathscr{D}(n_2^1, n_3^1) - n_1^1, r_{21}^2, \Delta, \mathscr{D}(n_2^2, n_3^2) - n_1^2]^T \in \mathbb{R}^3, \end{aligned} \tag{38}$$

where $\Delta = r_{11}^1 r_{31}^2 - r_{11}^2 r_{31}^1$. Note that the constraint $\Delta = 0$ imposes the restriction that the first column of R^1 and R^2, the gaze directions of the two eyes are coplanar with respect to the fixed vector $[0,1,0]^T$, which is the vector of separation between the centers of the eyes. Writing the dynamical system of the 'Binocular System' as a 6-input 6-output system defined on $\mathscr{N} \times \mathscr{N}$. The decoupling matrix N is written as follows:

$$\begin{bmatrix} 0 & -\frac{1}{J_2^1} r_{23}^1 & \frac{1}{J_3^1} r_{22}^1 & 0 & 0 & 0 \\ 0 & -\frac{1}{J_2^1} r_{33}^1 & \frac{1}{J_3^1} r_{32}^1 & 0 & 0 & 0 \\ L_{g_1} L_f h_3 & L_{g_2} L_f h_3 & L_{g_3} L_f h_3 & 0 & 0 & 0 \\ 0 & 0 & 0 & 0 & -\frac{1}{J_2^2} r_{23}^2 & \frac{1}{J_3^2} r_{22}^2 \\ 0 & \beta_1 & \beta_2 & 0 & \beta_3 & \beta_4 \\ 0 & 0 & 0 & L_{g_4} L_f h_6 & L_{g_5} L_f h_6 & L_{g_6} L_f h_6 \end{bmatrix}, \tag{39}$$

where $\beta_1 = (J_2^1)^{-1}[r_{13}^1 r_{31}^2 - r_{33}^1 r_{11}^2]$, $\beta_2 = (J_3^1)^{-1}[r_{32}^1 r_{11}^2 - r_{12}^1 r_{31}^2]$, $\beta_3 = (J_2^2)^{-1}[r_{31}^1 r_{13}^2 - r_{11}^1 r_{33}^2]$, and $\beta_4 = (J_3^2)^{-1}[r_{11}^1 r_{32}^2 - r_{31}^1 r_{12}^2]$. The determinant of the decoupling matrix N is given by

$$r_{11}^1 \left[J_2^1 J_3^1 J_2^2 J_3^2\right]^{-1} \left[L_{g_1} L_f h_3\right] \left[L_{g_4} L_f h_6\right] \left[r_{11}^1 r_{11}^2 + r_{31}^1 r_{31}^2\right]. \tag{40}$$

Let us now use the parametrization from (2) and describe the quaternion for the left eye using ψ_L, θ_L, ϕ_{1L} and for the right eye using ψ_R, θ_R, ϕ_{1R}. Using this notation, it is now easy to define Υ_L and Υ_R from (24), respectively for the left and the right eyes. The determinant of the decoupling matrix (39) can now be readily written as

$$\varsigma\,(1 + \tan\psi_L \tan\psi_R \cos\theta_L \cos\theta_R)\,\Upsilon_L \Upsilon_R, \tag{41}$$

where $\varsigma = \frac{1}{4}\,(J_1^1 J_2^1 J_3^1)^{-1}\,(J_1^2 J_2^2 J_3^2)^{-1}\,\cos^2\psi_L\,\cos\psi_R$. Note that (other than the points $\psi_L = \pi/2$ and $\psi_R = \pi/2$) the determinant (41) vanishes precisely on the Singularity surfaces (see (25)) $\Upsilon_L = 0$ and $\Upsilon_R = 0$ for the left and the right eyes respectively. Additionally the determinant vanishes on a 'mixed singularity surface'[9]

$$\Xi = 0, \tag{42}$$

where $\Xi = 1 + \tan\psi_L \tan\psi_R \cos\theta_L \cos\theta_R$. We remark that on the mixed singularity surface (42), the XZ projections[10] of the pointing directions of the two eyes are perpendicular to each other. In particular when both the eyes are either looking up or looking down, the mixed singularity condition is not satisfied.

Let us denote the Donders' surface (8), (23) for the left eye as $\mathscr{D}_L = 0$ and correspondingly for the right eye as $\mathscr{D}_R = 0$. We now write the coplanarity condition $\Delta = 0$ from (38) as

$$\tan\psi_R \cos\theta_R \;=\; \tan\psi_L \cos\theta_L. \tag{43}$$

The admissible region $\mathscr{N} \times \mathscr{N}$ are points satisfying the Donders' constraints together with the coplanarity condition (43). Note that the determinant (40) is nonzero in the admissible region, since $\left[r_{11}^1 r_{11}^2 + r_{31}^1 r_{31}^2\right]$ is nonzero, which is equivalent to requiring that $\Xi \neq 0$. The distance between the coplanarity surface (43) from the mixed singularity surface (42) shows in Fig. 5.

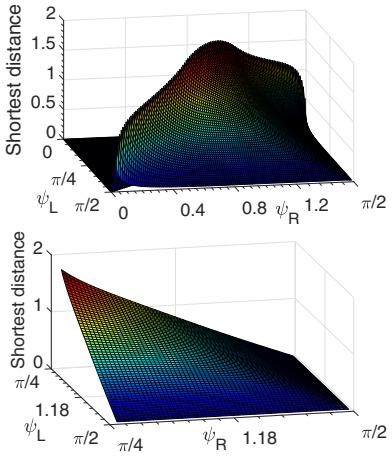

Fig. 5. For fixed value of ψ_L and ψ_R the shortest distance between the Coplanarity Surface (43) and the Mixed Singularity Surface (42) is plotted as ψ_L and ψ_R varies from 0 to the maximum possible value $\frac{\pi}{2}$. (left) ψ_L and ψ_R are assumed to take values $(\tan\psi_L \tan\psi_R) \geq 1$, where $\psi_L, \psi_R \leq \frac{\pi}{2}$, and (right) ψ_L and ψ_R takes values in the interval $\frac{\pi}{4} \leq \psi_L, \psi_R \leq \frac{\pi}{2}$.

[8] For each i, the underlying state space of the dynamical system (36), (37) is $\Xi = \mathscr{H}_{\Psi} \times \mathbb{R}^3$, a 6 dimensional manifold.

[9] Mixed singularity surface is described using coordinates from both the left and the right eye.

[10] This is the sagittal plane.

To end this section, we make this comment that the determinant of the Jacobian Matrix, for the binocular problem, is given by

$$64\,\cos^4\psi_L\,\cos^2\psi_R\,\sin\psi_L\,\sin\psi_R\,\left[\Xi\,\Upsilon_L\,\Upsilon_R\right]^2. \qquad (44)$$

As in the case of a single eye or head, it would follow by comparing (41) and (44) that, with the exception of points $\psi_L = 0$, $\psi_L = \frac{\pi}{2}$ and $\psi_R = 0$, $\psi_R = \frac{\pi}{2}$, the decoupling and the Jacobian matrices have identical singularity surfaces.

VIII. Results and Discussion

Dynamics of Eye and Head rotation can be viewed as an input/output system (9), (10). It was shown in [7] that in a neighborhood of the space $\mathscr{N}$ of allowed orientations constrained by Donders' and Listing's constraints, one can 'locally linearize' the 'rotation dynamics' (14a), (14b) by a static state feedback $u^* := a(x) + b(x)v$.

The main result of this paper is to estimate how big are the neighborhoods $\mathscr{N}$ over which the dynamics can be linearized. It turns out, using a theorem due to Hadamard [19], that the size of the neighborhoods depend on the distance of the Singularity Surface (28) from the space $\mathscr{N}$ where the states of the dynamics, constrained by Donders' surface, nominally belong. These surfaces have been plotted, for four different choices of the Donders' surface parameters, in Fig. 1 for fixed values of ψ. Distance between the surfaces are plotted in Fig. 2 as a function of ψ, where it is assumed that ψ varies from 0 to $\bar{\psi}$. The distance plots have been generalized in Fig. 4b wherein we have obtained a lower bound between the Donders' surface and the Singularity surface assuming arbitrary parameters of the Donders' polynomial (5).

The other major result of this paper is to extend the feedback linearization construction from [7] to 'dynamics of binocular vision' (36), (37). We assume that the centers of the two eyes remain fixed, and nominally their gaze directions always meet at a point. We also assume that the two eyes satisfy the same Donders' condition. Our main result is that the binocular dynamics is feedback linearizable if the states of the two eyes are separately, away from their respective singularity surfaces $\Upsilon_L = 0$ and $\Upsilon_R = 0$ and if the 'projections of the gaze directions of the two eyes on the XZ plane (saggital plane) are not perpendicular to each other.' The two eyes are nominally on the surface where their gaze directions meet at a point, we call this the coplanarity surface. In Fig. 5, we plot the distance between the coplanarity surface (43) from the mixed singularity surface (42). For the feedback linearization to work, the gaze directions are allowed to perturb but their sagittal plane projections are not allowed to be perpendicular to each other. What we observe, in particular, is that when ψ_L and ψ_R is such that $\tan\psi_L \tan\psi_R < 1$ no perturbation of the other angle variables would touch the mixed singularity surface. For other cases, one has to refer to the distance plots in Fig. 5. From the distance functions plotted in Figs. 2, 3, 4 and 5, it is now easy to construct semiglobal neighborhoods on which feedback linearization is possible for single or binocular eye and head movement dynamics. Individual eyes have to **separately maintain separation between the Donders' and the Singularity surfaces**. The binocular eye, additionally, has to **maintain separation between the coplanarity and the mixed singularity surfaces**. All distance plots are sketched in this paper. Additionally a lower bound function (sketched as a surface) on the shortest distance between the Donders' and the Singularity surface has been sketched for a general class of Donders' surfaces.

References

[1] D. Robinson, "The mechanics of human saccadic eye movement," *The Journal of physiology*, vol. 174, no. 2, pp. 245–264, 1964.

[2] G. C. Peng, T. C. Hain, and B. W. Peterson, "Predicting vestibular, proprioceptive, and biomechanical control strategies in normal and pathological head movements," *Biomedical Engineering, IEEE Transactions on*, vol. 46, no. 11, pp. 1269–1280, 1999.

[3] B. K. Ghosh, I. Wijayasinghe, and S. D. Kahagalage, "A geometric approach to head/eye control," *IEEE Access*, vol. 2, pp. 316–332, 2014. [Online]. Available: http://dx.doi.org/10.1109/ACCESS.2014.2315523

[4] W. Medendorp, J. Van Gisbergen, M. Horstink, and C. Gielen, "Donders' law in torticollis," *Journal of neurophysiology*, vol. 82, no. 5, pp. 2833–2838, 1999.

[5] D. Tweed, "Three-dimensional model of the human eye-head saccadic system," *Journal of Neurophysiology*, vol. 77, no. 2, pp. 654–666, 1997.

[6] I. Wijayasinghe, J. Ruths, U. Büttner, B. K. Ghosh, S. Glasauer, O. Kremmyda, and J.-S. Li, "Potential and optimal control of human head movement using Tait-Bryan parametrization," *Automatica*, vol. 50 (2), pp. 519–529, 2014.

[7] T. Oki and B. K. Ghosh, "A transverse local feedback linearization approach to human head movement control," *Control Theory and Technology*, vol. 15, no. 4, pp. 245–257, 2017.

[8] A. D. Polpitiya, W. P. Dayawansa, C. F. Martin, and B. K. Ghosh, "Geometry and control of human eye movements," *Automatic Control, IEEE Transactions on*, vol. 52, no. 2, pp. 170–180, 2007.

[9] A. J. Hanson, *Visualizing Quaternions*. Morgan Kaufmann, 2006.

[10] A. Novelia and O. M. O'Reilly, "On geodesics of the rotation group SO(3)," *Regular and Chaotic Dynamics*, vol. 20, no. 6, pp. 729–738, 2015.

[11] ——, "On the dynamics of the eye: geodesics on a configuration manifold, motions of the gaze direction and helmholtzs theorem," *Nonlinear Dynamics*, vol. 80, no. 3, pp. 1303–1327, 2015.

[12] O. Kremmyda, S. Glasauer, L. Guerrasio, and U. Büttner, "Effects of unilateral midbrain lesions on gaze (eye and head) movements," *Ann. N. Y. Acad. Sci.*, vol. 1233, pp. 71–77, 2011.

[13] S. Glasauer, M. Hoshi, U. Kempermann, T. Eggert, and U. Büttner, "Three dimensional eye position and slow phase velocity in humans with downbeat nystagmus," *J. Neurophysiol.*, vol. 89, pp. 338–354, 2003.

[14] O. M. O'Reilly, *Intermediate dynamics for engineers*. Cambridge University Press, New York, NY, 2008.

[15] N. A. Chaturvedi, A. K. Sanyal, and N. H. McClamroch, "Rigid-body attitude control," *Control Systems, IEEE*, vol. 31, no. 3, pp. 30–51, 2011.

[16] A. Isidori, *Nonlinear Control Systems, 3rd edition*. Springer, 1995.

[17] C. Nielsen and M. Maggiore, "On local transverse feedback linearization," *SIAM Journal on Control and Optimization*, vol. 47, no. 5, pp. 2227–2250, 2008.

[18] C. Nielsen, C. Fulford, and M. Maggiore, "Path following using transverse feedback linearization: Application to a maglev positioning system," *Automatica*, vol. 46, no. 3, pp. 585–590, 2010.

[19] M. S. Berger, *Nonlinearity and Functional Analysis: Lectures on Nonlinear Problems in Mathematical Analysis*. Academic Press, 1977.

[20] B. Athukorallage and B. K. Ghosh, "Human head and binocular eye movement control via feedback linearization," in *Proc. of the 2018 American Control Conference (ACC)*, 2018.